The Bromide-Bromomethyl Radical Dimer Complex: Anion Photoelectron Spectroscopy and CCSD(T) Calculations

Christian T. Haakansson, Timothy R. Corkish, Peter D. Watson, Allan J. McKinley & Duncan A. Wild*

School of Molecular Sciences, The University of Western Australia, Crawley, Western Australia, 6009, Australia

**duncan.wild@uwa.edu.au +61 8 6488 3178*

Abstract

The gas phase anion photoelectron spectrum associated with the bromide-bromomethyl radical is presented. The stabilisation energy and electron binding energy, a property corresponding to the electron affinity of the neutral complex, are determined. *Ab initio* MP2 optimisations (with additional CCSD(T) energies) found two forms of the complex, a hydrogen bonded complex and a halogen bonded complex. The halogen bonded complex was found to exhibit C_{2v} symmetry and the hydrogen bonded complex exhibited C_s symmetry. Comparison between the experimental data and the computational data allow conclusions to be drawn about the structure of the experimentally observed species.

Keywords: photoelectron spectroscopy, gas phase anions, dibromomethane, mass spectrometry.

1 Graphical Abstract

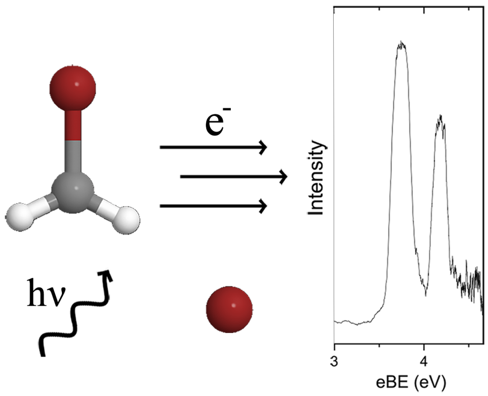

2 Introduction

Halogenated methanes readily undergo dissociative electron attachment, in large part due to the significant electron affinity associated with the halogen atoms [1]. Dibromomethane, which has a large rate constant of thermal electron capture [2, 3], is such an example and undergoes dissociative electron attachment to produce a bromide anion and bromomethyl radical [1,4]. Following the electron capture and resultant dissociation of dibromomethane, the nascent bromide anion and bromomethyl radical can form a loosely-bound van der Waals complex.

The resultant bromide-bromomethyl radical complex ($Br^- \cdots CH_2Br\cdot$) features the bromide anion bound either to a single hydrogen of the bromomethyl radical or bound linearly to the bromine atom of the bromomethyl radical. This system has previously been the subject of study by means of infrared spectroscopy [5]. It was determined that the predominant form of the complex sees the bromide bound to the bromomethyl radical through a single hydrogen bond, whilst the bromine bound system was found to be higher in energy and not spectroscopically observed [5]. The binding displayed in the hydrogen bound complex was found to be similar to the style of binding observed in the iodide-methyl radical ($I^- \cdots CH_3\cdot$) system, where the iodide appends to a single hydrogen of the methyl radical [5, 6].

As was suggested above, the bromide-bromomethyl radical complex can also feature the bromide appended linearly to the bromine atom of the bromomethyl radical. This type of arrangement is highly similar to that observed in the chloride - trichloromethyl radical ($H_2O \cdots Cl^- \cdots CCl_3\cdot$) system where the chloride anion binds linearly to a single chlorine of the trichloromethyl radical moeity [7]. This structural motif is also observed for chloride-tetrachloromethane ($Cl^- \cdots CCl_4$), where the chloride anion binds linearly to a single chlorine atom of the tetrachloromethane moeity [8]. This binding is termed a halogen bond where the negatively charged halide forms a stabilising interaction with the σ-hole located on the halogen atom of the molecular moeity [9]. The halogen bond is thought to be comprised of electrostatic and polarization Coulombic terms [10, 11], as well as some contribution from charge transfer [12, 13].

Anion photoelectron spectroscopy is a technique that allows elucidation of properties associated with a neutral species based on photoelectron detachment from an anion, with recent examples provided here [14–16]. The technique can be easily extended to the study of ion-molecule van der Waals complexes including radical containing complexes such as $I^- \cdots CH_3\cdot$ [6] and $I^- \cdots H_2O \cdots CH_2CH_3\cdot$ [17]. The major information provided by anion photoelectron spectroscopy is the electron binding energy associated with the complex, with increased resolution able to reveal the vibrational states of the associated neutral species [18].

The power of anion photoelectron spectroscopy in relation to charged van der Waals complexes is observation of the increase in electron binding energy of the complexed system with respect to that of the bare anion, which results in information related to the strength of the bonding. As an illustrative example, a photoelectron spectrum of a bare bromide anion yields a $^2P_{3/2}$ photodetachment peak at approximately $3.36\,\mathrm{eV}$ [19, 20], when complexed with a nitrogen molecule (*i.e.* $\mathrm{Br^-\cdots N_2}$) the $^2P_{3/2}$ photodetachment peak associated with bromide shifts to approximately $3.43\,\mathrm{eV}$ [21]. In contrast, the complex formed between bromide and water (*i.e.* $\mathrm{Br^-\cdots H_2O}$) shifts the $^2P_{3/2}$ photodetachment peak associated with bromide to $3.93\,\mathrm{eV}$ [22], which shows the stronger ion-dipole interaction between bromide and water that leads to a larger stabilisation of the negative charge, thus shifting the photodetachment peak to higher energy.

In this paper, we present the photoelectron spectrum assigned to a gas phase van der Waals complex consisting of bromide and a bromomethyl radical. The structure of this complex has been refined using *ab initio* calculations, with the photoelectron detachment energies simulated using CCSD(T) single point energy calculations.

3 Methods

3.1 Experimental Methods

The experimental work associated with this research was performed using a time-of-flight anion mass spectrometer in tandem with a time-of-flight photoelectron spectrometer (TOF-PES). The mass spectrometer allows mass selection of desired anion complexes of interest and is based on the Wiley-McLaren design [23]. The mass spectrometer is coupled to a magnetic bottle style photoelectron spectrometer based on the design of Cheshnovsky *et al* [24]. The overall experimental setup associated with the Wild group has been described in detail previously [25], and therefore only specific experimental parameters associated with the current work are detailed here.

The experimental gas mixture associated with the experiment consisted of dibromomethane and argon with a total pressure of $400\,\mathrm{kPa}$, with the gas mixture consisting almost entirely of argon. The dibromomethane was introduced into the gas mixture by way of its vapour pressure. The gas mixture was then pulsed through a piezo-electric nozzle and intersected by a stream of energetic electrons from a Rhenium filament. The anion van der Waals complexes of interest then form following dissociative electron attachment processes. The $\mathrm{Br^-\cdots CH_2Br\cdot}$ complex is then mass selected from the associated time-of-flight and intersected by a $5\,\mathrm{ns}$ pulse of $266\,\mathrm{nm}$ $(4.66\,\mathrm{eV})$ laser radiation (fourth harmonic of a Nd:YAG Spectra Physics Quanta Ray Pro). The photodetached electrons are then captured in a strong divergent magnetic field and guided to the photoelectron detector by a homogenous solenoid magnetic field along a $1.8\,\mathrm{m}$ flight tube, the divergent magnet acting in unison with the solenoid magnetic field is what constitutes the magnetic bottle design. The photoelectron time-of-flight was then recorded and, upon conversion to kinetic energy (eKE), used to determine the electron binding energy (eBE) associated with the $Br^{-} \cdots CH_2Br\cdot$ complex by way of the known photon energy ($h\nu$) via Eq. 1.

$$eBE = h\nu - eKE \tag{1}$$

Conversion from photoelectron time-of-flight to kinetic energy is not a linear process, and therefore involves a Jacobi transform rescaling the spectral intensity with respect to energy as opposed to time-of-flight. Essentially, the Jacobi transform is performed by multiplying the spectral intensity with respect to time-of-flight with the time-of-flight cubed (t^3). In order to observe an appreciable photoelectron signal associated with $Br^{-} \cdots CH_2Br\cdot$, multiple spectra were recorded and averaged with each photoelectron spectrum consisting of 10000 laser shots. In addition to recording the photoelectron spectrum of the $Br^{-} \cdots CH_2Br\cdot$ complex, calibration spectra were recorded for bare bromide and iodide, with iodide present from previous experiments. The known energy of the $^2P_{3/2}$ and $^2P_{1/2}$ spin-orbit states associated with detachment from both bromide and iodide allow calibration between time-of-flight and kinetic energy.

3.2 Computational Methods

The geometry associated with the bromide-bromomethyl radical complex was optimised at the MP2 level of theory in the Gaussian 09 software package [26]. Dunning's augmented, correlation consistent basis sets were employed, with carbon and hydrogen allocated their respective aug-cc-pVQZ (AVQZ) basis sets [27, 28]. With respect to bromine, the corresponding pseudo-potential basis set of the form aug-cc-pVQZ-PP (AVQZ) was employed [29]. The geometry optimisations were followed by vibrational analyses at the associated level of theory in order to ensure the optimised geometry constituted a minimum on the potential energy surface. Owing to the relatively weak binding exhibited by these van der Waals complexes, strict convergence criteria were employed ($1 * 10^{-8} E_h a_0^{-1}$).

Following on from the MP2/AVQZ optimisation and associated harmonic vibrational analysis of the bromide-bromomethyl radical complex, single point energies were computed at the MP2/AV5Z level of theory as well as using the CCSD(T) method. All CCSD(T) calculations were carried out using the CFOUR software package [30]. The final energies associated with the complex, and the ones presented here, represent complete basis set (CBS) energies. Two complete basis set extrapolation methods were employed: the first involving the MP2 energies and the second involving the CCSD(T) energies. With respect to the MP2 energies, the SCF energy was extrapolated based on AVQZ and AV5Z energies using the formula of Karton and Martin [31], which can be seen in Eq. 2.

$$E_\infty = E_L + \frac{E_L - E_{L-1}}{\frac{Lexp(9(\sqrt{L}-\sqrt{L-1}))}{L+1} - 1} \tag{2}$$

In contrast, the MP2 correlation energy was extrapolated based on the AVQZ and AV5Z energies using the formula of Eq. 3. With respect to the MP2 energies, a value of $\alpha = 3$ was used in accordance with Helgaker *et al* [32]. The CCSD(T) energies were extrapolated following the W1w protocol [33], again making use of Eq. 3. The W1w protocol requires extrapolation of the SCF energy from the AVTZ energy and the AVQZ energy with $\alpha = 5$ [34]. The CCSD energy contribution is similarly extrapolated, but with $\alpha = 3.22$ [34]. In contrast, the pertubative triples (T) energy contribution is extrapolated from the AVDZ energy and the AVTZ energy with $\alpha = 3.22$ [34].

$$E_\infty = E_L + \frac{E_L - E_{L-1}}{(\frac{L}{L-1})^\alpha - 1} \tag{3}$$

In order to investigate the planarity of the bromomethyl radical and the bromdie-bromomethyl radical complex, relaxed potential energy scans were employed. These potential energy scans involved the use of B3LYP [44], MP2 and CCSD(T) methods all using the AVTZ basis set. The CCSD(T)/AVTZ scan involved single point energy determinations at this level of theory based on optimised geometries at the MP2/AVTZ level of theory (*i.e.* the CCSD(T)/AVTZ//MP2/AVTZ level of theory).

4 Results & Discussion

4.1 Computational Results

4.1.1 Theoretical Complex Geometries

Prior to consideration of the van der Waals complex formed between a bromide anion and a bromomethyl radical, first we shall consider the bromomethyl radical moeity in isolation. The bromomethyl radical is part of a family of monosubstituted halomethyl radicals consisting of the fluoromethyl, the chloromethyl, the bromomethyl, and the iodomethyl radicals. These species have been the subject of spectroscopic study and it has been found moving through the series that the fluoromethyl radical is quasiplanar [35], while the chloromethyl [36], bromomethyl [37, 38], and iodomethyl radicals are planar [39]. This trend has been attributed to the decreasing electronegativity of the halogen atom along the series [40]. Therefore, based on experimental investigation, the bromomethyl radical is considered to be planar. When studied computationally, the planarity of the radical at first appears inconsistent with optimisation of planar and near-planar structures depending on the method and basis set used [41–43]. However, as has been noted in a previous *ab initio* study, there appears to be no substantial difference between the near-planar and planar structures when comparing their respective calculated properties [41]. The bromomethyl radical was optimised as part of this study and found to be near planar at the MP2/AVQZ level of theory, with a dihedral angle of $2.8°$. A subsequent relaxed potential energy scan was performed, scanning the dihedral angle at the B3LYP/AVTZ level of theory as well as CCSD(T)/AVTZ single point energies based on MP2/AVTZ optimised points (*i.e.* the CCSD(T)/AVTZ//MP2/AVTZ level of theory). Overlayed on the scan is the zero-point energy associated with the inversion mode of the radical, which can be seen in Figure 1. With reference to the scan, a minor inversion barrier can be seen associated with both the MP2 and CCSD(T) results. However, the zero-point energy of the inversion mode places the ground state above the inversion barrier, which renders the vibrationally averaged structure of the radical planar.

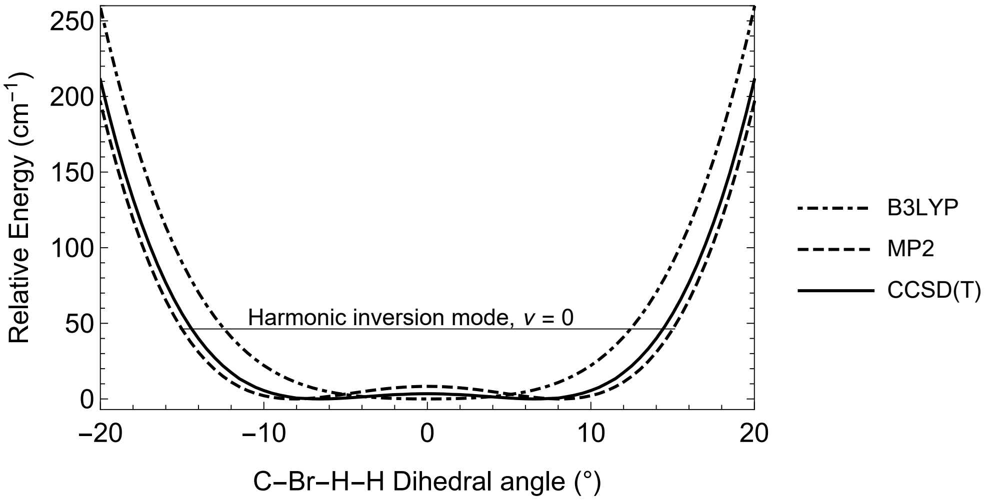

Figure 1: Relaxed scan of the C-Br-H-H dihedral angle of the bromomethyl radical, performed at B3LYP/AVTZ (dot-dashed line), MP2/AVTZ (dashed line) and CCSD(T)/AVTZ//MP2/AVTZ (solid line). The zero-point energy associated with the inversion mode has been shown using a solid line. (Note: the inversion mode was determined using the harmonic approximation at the MP2/AVQZ level of theory.)

The bromide-bromomethyl radical complex geometries have been optimised at the MP2/AVQZ level of theory with the associated vibrational analysis resulting in all real modes. As was suggested earlier, two geometries of the complex exist, one with the bromide anion appended to a single hydrogen of the bromomethyl radical moeity and one with the bromide anion appended linearly to the bromine atom of the bromomethyl radical moeity; these two structures will be referred to as the hydrogen bonded and halogen bonded geometries respectively. The hydrogen bonded geometry displayed C_1 symmetry (Figure 2. a), whereas the halogen bonded geometry displayed C_{2v} symmetry (Figure 2. b). The hydrogen bonded geometry exhibited the bromide anion bound at a distance of approximately $2.42\,\text{Å}$ with respect to the hydrogen and with an angle of $168°$ with respect to the C – H bond. The halogen bonded geometry on the other hand, featured the bromide anion bound linearly at a distance of approximately $3.22\,\text{Å}$ with respect to the bromine atom.

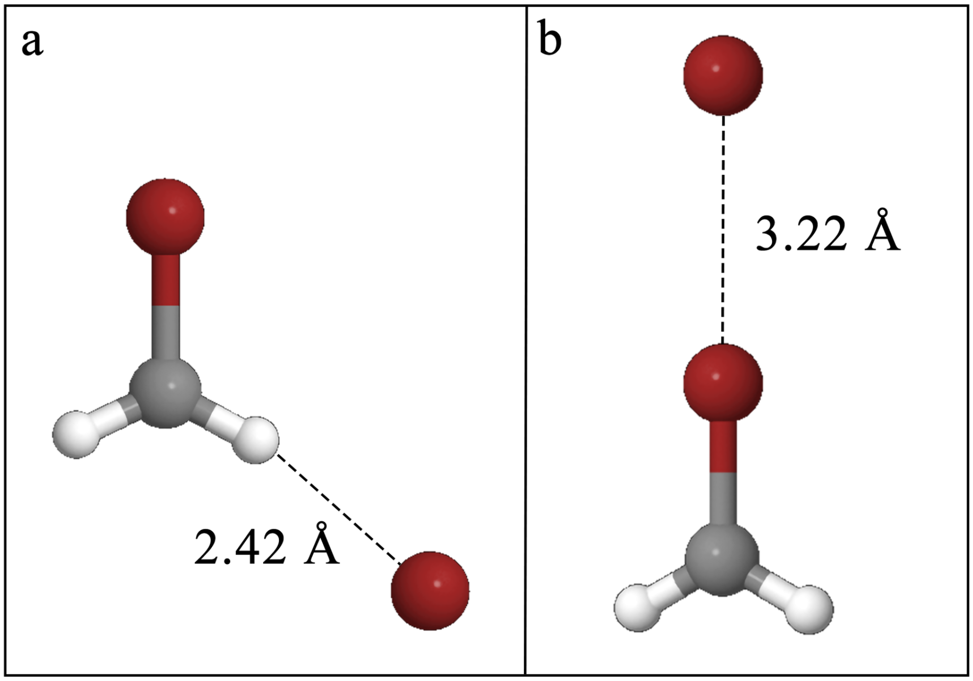

Figure 2: MP2/AVQZ predicted geometries of the bromide-bromomethyl radical complex; a. represents the hydrogen bonded geometry and b. represents the halogen bonded geometry.

The bare bromomethyl radical has C – H bond distances of $1.072\,\text{Å}$ and a C – Br bond distance of $1.827\,\text{Å}$. As shown by way of Figure 1, the bare bromomethyl radical is planar, but when complexed with a bromide anion, the bromomethyl radical undergoes minor structural changes. With respect to the halogen bonded geometry, this complex was found to be planar with the C – Br bond elongating to a distance of $1.833\,\text{Å}$. In terms of the hydrogen bonded geometry, the C – H bond with which the bromide anion interacts elongates increasing from $1.072\,\text{Å}$ to $1.088\,\text{Å}$. A scan similar to that performed for the bare bromomethyl radical was performed for the hydrogen bound complex, and is provided in Figure 3. In contrast to the bare bromomethyl radical, a B3LYP/AVTZ scan was not performed with respect to the complex, since results associated with the B3LYP functional have been found unreliable with respect to loosely bound complexes [45]. The dihedral angle scan associated with the hydrogen bound complex tells a similar story to that of the bare bromomethyl radical; where high level *ab initio* results suggests a near planar geometry, however once again the zero-point energy of the inversion mode places the ground state above the inversion barrier, again resulting in the vibrationally averaged structure being planar in the ground state configuration. It is worth noting that the inversion barrier at the CCSD(T)/AVTZ//MP2/AVTZ level of theory associated with the bare radical is approximately $4\,\text{cm}^{-1}$, whereas the inversion barrier associated with the hydrogen bound complex increases to approximately

$12\,\mathrm{cm}^{-1}$. Based on the difference in inversion barrier, the out-of-plane geometry can be said to be more pronouced in the hydrogen bound complex. However, since the inversion mode undergoes blueshift to higher energy, the ground state of the hydrogen bound complex still lies far above the inversion barrier. Therefore, the vibrationally averaged ground state of the hydrogen bonded complex exhibits C_s symmetry.

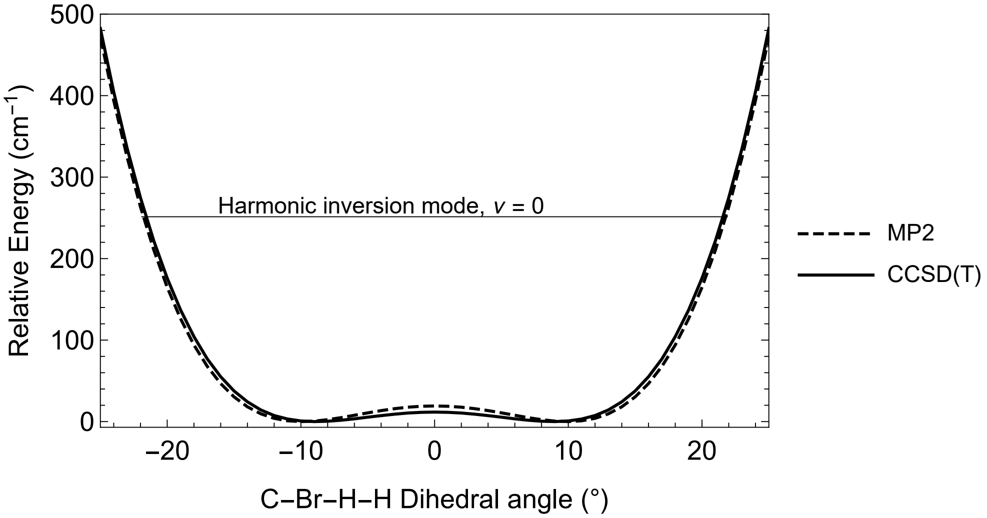

Figure 3: Relaxed scan of the internal bromomethyl radical dihedral angle (*i.e* the C-Br-H-H dihedral angle) associated with the hydrogen bonded bromide-bromomethyl radical complex, performed at MP2/AVTZ (dashed line) and CCSD(T)/AVTZ//MP2/AVTZ (solid line). The zero-point energy associated with the inversion mode has been shown using a solid line. (Note: the inversion mode was determined using the harmonic approximation at the MP2/AVQZ level of theory.)

A comparison of the equilibrium and harmonic dissociation energies (*i.e.* D_e and D_0) with respect to the two geometries is presented in Table 1. Importantly, the dissociation energies show the hydrogen bonded geometry to be more stable than the halogen bonded geometry by approximately $12.9\,\mathrm{kJ/mol}$. The relative dissociation energies suggest that experimental observation of the halogen bonded geometry is unlikely, indeed a simple Boltzmann distribution shows that the relative population of the halogen bonded geometry at $298\,\mathrm{K}$ would approach $0.54\,\%$ and be even less at experimental temperatures in a molecular beam produced via supersonic expansion. As seen in Table 1, the dissociation energies have been determined both at the MP2/CBS and CCSD(T)/CBS levels of theory. In general, there is a high degree of agreement between the two levels of theory, with the MP2 results appearing to slightly underestimate the strength of the hydrogen bonded system and slightly overestimating the strength of the halogen bonded system, with respect to the CCSD(T)/CBS results.

Table 1: Dissociation energies of the hydrogen bonded and halogen bonded bromide-bromomethyl radical complexes. The equilibrium dissociation energy (D_e) and harmonic dissociation energy (D_0) have been calculated both at the MP2/CBS and the CCSD(T)/CBS levels.

$Br^{-} \cdots CH_2Br \cdot$	D_e [kJ/mol]		D_0 [kJ/mol]	
	MP2	CCSD(T)	MP2	CCSD(T)
Hydrogen bonded	38.5	39.2	35.9	36.6
Halogen bonded	25.6	24.9	24.4	23.7

4.1.2 Predicted Vertical Detachment Energies

The Franck-Condon principle dictates that the most intense transition in an anion photoelectron spectrum will be the vertical detachment transition where an electron is instantaneously detached and the complex retains the anion geometry. The vertical detachment energy was predicted by determining the difference in energy of the anion geometry and a neutral complex at the anion geometry, thereby simulating the instantaneous release of a photoelectron. The vertical detachment energy was computed at both the CCSD(T)/CBS and MP2/CBS levels of theory based on the MP2/AVQZ optimised geometry associated with the anion complex in question. **The anion state is a doublet anion and the photodetachment event results in the loss of a sinlge electron from the bromide anion, resulting in the production of a bromine radical. The resultant system formed by way of instantaneous photoelectron detachment would exist either as a triplet biradical or a singlet biradical.**

The predicted vertical detachment energies associated with both the singlet and the triplet states are provided in Table 2. Given both singlet and triplet states involves detachment of an electron from the bromide anion, in order to gain an accurate estimate of the transition energy, the raw computational energies need to be split in accordance with the spin-orbit states of bromine as this is not included computationally. Therefore in order to allow determination of the detachment transitions associated with the $^2P_{3/2}$ and $^2P_{1/2}$ states of bromine, the experimental coupling constant associated with bromine was added. **Due to the loose nature of the binding between the bromide anion and the bromomethyl radical, the spin-orbit constant associated with the bromomethyl radical moeity was not included since the detached electron originated from the bromine radical. Additionally, the spin-orbit constant associated with a bromomethyl radical is approximately $415\,\mathrm{cm}^{-1}$ [37], which is much less than that of bromine.** A further shift was applied to the computational results based on the difference between MP2/CBS and CCSD(T)/CBS energies associated with the computed bare halide transitions and those associated with the corresponding experimental transitions. In practice, that translates to a shift of $-0.107\,\mathrm{eV}$ added to the MP2/CBS energy and a shift of $-0.013\,\mathrm{eV}$ added to the CCSD(T)/CBS energy.

Table 2: Summary of the singlet and triplet vertical detachment energies (VDE) determined for both the hydrogen and halogen bonded complexes.

Hydrogen Bonded		CCSD(T)/CBS [eV]	MP2/CBS [eV]
Singlet VDE	$^2P_{3/2}$	4.07	4.52
	$^2P_{1/2}$	4.53	4.98
Triplet VDE	$^2P_{3/2}$	3.74	3.76
	$^2P_{1/2}$	4.19	4.21
Halogen Bonded		CCSD(T)/CBS [eV]	MP2/CBS [eV]
Singlet VDE	$^2P_{3/2}$	3.59	3.58
	$^2P_{1/2}$	4.04	4.04
Triplet VDE	$^2P_{3/2}$	3.59	3.59
	$^2P_{1/2}$	4.04	4.04

With reference to Table 2, the vertical detachment energies associated with the triplet state show a high level of agreement between the respective MP2/CBS and CCSD(T)/CBS values. **This is not the case for the singlet biradical detachment state where a mismatch between MP2 and CCSD(T) can be seen,** this mismatch is particularly evident associated with the singlet detachment state of the **hydrogen** bonded complex and could point to the requirement of multi-reference methods in order to accurately determine the energy of this state. The singlet **biradical** state was not further explored and is beyond the scope of this work, since as is shown by the experimental photoelectron spectrum in Figure 5, the experimental energies were found to be in excellent agreement with the triplet state vertical detachment energies associated with the hydrogen bonded complex.

4.2 Experimental Results

4.2.1 Mass Spectrometry

A typical mass spectrum associated with the dibromomethane and argon gas mixture can be seen in Figure 4. The bare halide peaks in the mass spectrum occur at $79\,\mathrm{m/z}$, $81\,\mathrm{m/z}$ and $127\,\mathrm{m/z}$, the characteristic splitting pattern associated with the $79\,\mathrm{m/z}$ and $81\,\mathrm{m/z}$ peaks being that of bromide. Iodide occurs as a singular peak at $127\,\mathrm{m/z}$. The cluster of peaks located at $172\,\mathrm{m/z}$, $174\,\mathrm{m/z}$ and $176\,\mathrm{m/z}$, indicated by the asterisk, result from the bromide-bromomethyl radical complex. The characteristic splitting of these peaks in an isotopic ratio of approximately 1:2:1 occurs as a result of the complex containing two bromine atoms, each of which have their intrinsic isotopic splitting of approximately 1:1.

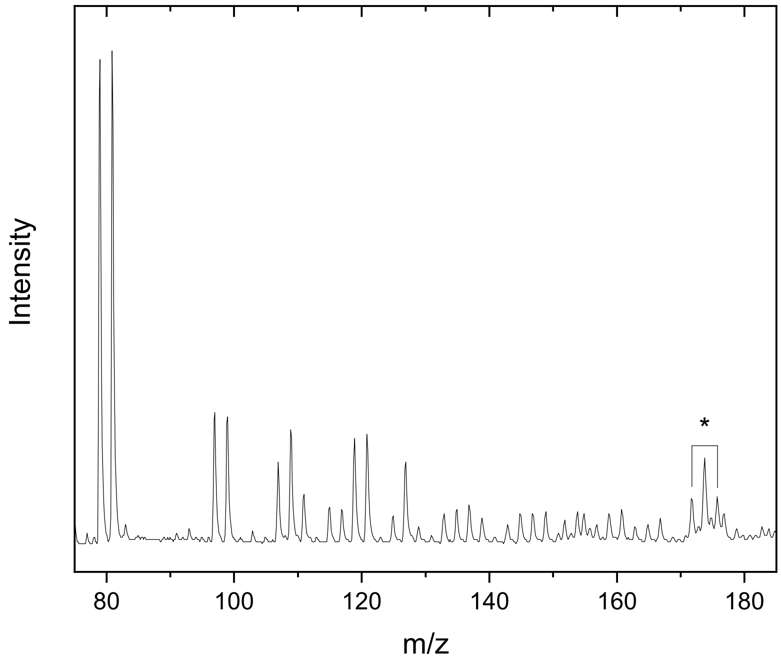

Figure 4: Experimental mass spectrum associated with a gas mixture containing argon, and dibromomethane. The envelope asterisk indicates the triplet of peaks associated with the bromide-bromomethyl radical complex.

In addition to the bare halide peaks and the peaks associated with the bromide-bromomethyl radical complex, other peaks were also present. The complex formed between bromide and water was observed at $97\,\mathrm{m/z}$ and $99\,\mathrm{m/z}$, whilst the complex formed between bromide and nitrogen was observed at $107\,\mathrm{m/z}$ and $109\,\mathrm{m/z}$. The complex formed between bromide and argon, the other component of the experimental gas mixture, was observed at $119\,\mathrm{m/z}$ and $121\,\mathrm{m/z}$. The doublet oberserved at $109\,\mathrm{m/z}$ and $111\,\mathrm{m/z}$ is attributed to the bromide-formaldehyde complex, with formaldehyde a remnant from a previous experiment.

4.2.2 Photoelectron Spectroscopy

The photoelectron spectrum of the bromide-bromomethyl radical complex can be seen in Figure 5, with the associated electron binding energies tabulated in Table 3. The electron stabilisation energy (E_{stab}) refers to the difference in binding energy with respect to the bare bromide anion and the bromide-bromomethyl radical complex.

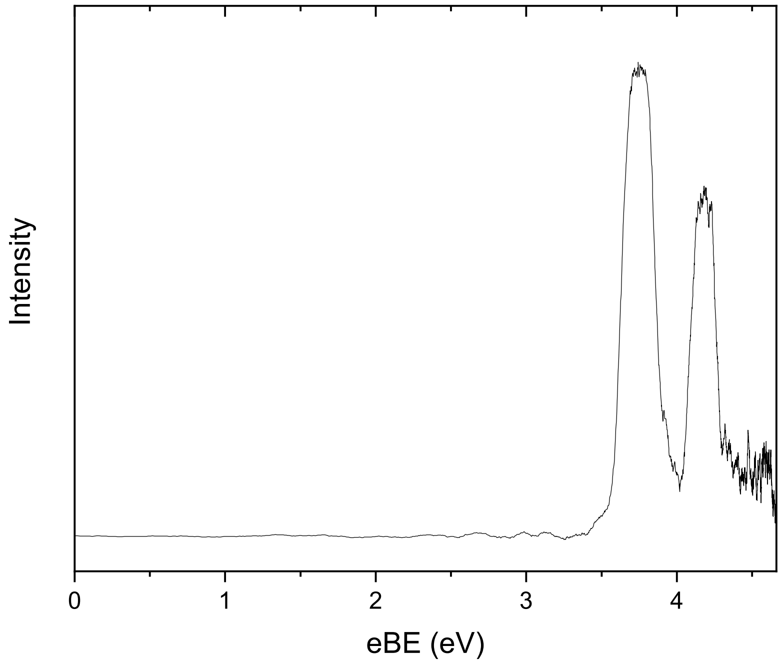

Figure 5: Experimental photoelectron spectrum of the bromide-bromomethyl radical system recorded using a photon energy of $4.66\,\mathrm{eV}$.

In the photoelectron spectrum, the main observable feature is the two peaks corresponding to the two spin-orbit states of bromine (*i.e.* $^2P_{3/2}$ and $^2P_{1/2}$). The observation of the two spin-orbit states of bromine confirm the identity of the species as a van der Waals complex consisting of a bromide anion loosely bound to a bromomethyl radical, rather than a molecular anion. This agrees with the idea that anion photoelectron spectra involving van der Waals complexes can generally be thought of as a pertubation of the corresponding photoelectron spectrum of the bare anion [46]. As mentioned previously, the computed energies associated with detachment to the triplet state of the hydrogen bonded complex are in excellent agreement with the experimentally determined peaks. The presence of peaks associated with the halogen bonded species cannot be ruled out as the calculated positions would suggest their being convoluted within the major peaks associated with the hydrogen bonded complex. The minor shoulder on the main $^2P_{3/2}$ peak at around $3.6\,\mathrm{eV}$ could be the result of $^2P_{3/2}$ peak associated with the halogen bonded complex, which was calculated to occur at $3.59\,\mathrm{eV}$. However, given the resolution of the experimental spectrum combined with the outcome of the Boltzmann distribution, this assignment is not appropriate. Therefore, the major form of the complex was found to be the hydrogen bonded form, which is in agreement with a previous infrared spectroscopic study of the complex [5].

Table 3: Experimentally determined binding energies associated with the $^2P_{3/2}$ and $^2P_{1/2}$ photodetachment states of a bare bromide anion and the bromide-bromomethyl radical complex. The computationally determined vertical detachment energy associated with the hydrogen bonded geometry has been provided in italics.

	$^2P_{3/2}$ [eV]	$^2P_{1/2}$ [eV]	E_{stab} [eV]
Br^-	3.35	3.82	-
$\mathrm{Br}^- \cdots \mathrm{CH_2Br}\cdot$	3.75	4.18	0.40
$\mathit{Br}^- \cdots \mathit{CH}_2\mathit{Br}\cdot$	*3.74*	*4.19*	-

5 Conclusion

Two geometries associated with the bromide-bromomethyl radical complex were optimised at the MP2/AVQZ level of theory with associated energetics determined at the CCSD(T)/CBS level of theory. Dissociation energies were determined with respect to each form of the complex and the hydrogen bonded form was found to be more stable, with a dissociation energy of $36.6\,\mathrm{kJ/mol}$. Initially, the computed structures of the bare bromomethyl radical appeared to deviate from the known planar structure. However, potential energy scans at different levels of theory showed the radical to be planar in the vibrationally averaged ground state. Similarly, the hydrogen bonded complex was found to be planar in the ground state from potential energy scans. The hydrogen bonded complex was found to exihibit C_s symmetry whilst the halogen bonded complex was found to exhibit C_{2v} symmetry.

The photoelectron spectrum associated with the bromide-bromomethyl complex was presented and characterised by the two major photodetachment peaks of bromine occurring at $3.75\,\mathrm{eV}$ and $4.18\,\mathrm{eV}$ respectively. These peak locations were found to be in excellent agreement with the computed detachment peaks of the hydrogen bonded complex, found to occur at $3.74\,\mathrm{eV}$ and $4.19\,\mathrm{eV}$ respectively. Overall, the experimental data combined with the computational data show the hydrogen bonded complex to be by far the most abundant. However, the presence of photodetachment peaks attributed to the halogen bonded complex cannot be discounted as they would likely be convoluted within the main peaks.

6 Acknowledgements

This research was undertaken with the assistance of computational resources from the Pople high-performance computing cluster of the Faculty of Science at the University of Western Australia. The Australian Research Council is acknowledged for funding the laser installation under the LIEF scheme (LE110100093). The School of Molecular Sciences and the Faculty of Science are acknowledged for financial support. C.

T. H. acknowledges the UWA Dean's Excellence in Science PhD Scholarship, while T. R. C. thanks the support of an Australian Government Research Training Program (RTP) scholarship.

7 Supplementary Information

- In depth energetics, vibrational modes and cartesian coordinates of the bromide-bromomethyl radical complexes.

8 References

[1] Schramm, A.; Ruf, M-W.; Matejcik, S.; Fabrikant, I. I.; Hotop, H. High-resolution study of dissociative electron attachment to dipolar molecules at low energies: CH_2Br_2 and CCl_3Br. *J. Phys. B*. **2002**, *35*, 4179-4202. DOI: 10.1088/0953-4075/35/20/306

[2] Sunagawa, T.; Shimamori, H. Low-energy electron attachment to brominated methanes. *J. Chem. Phys.* **1997**, *107*, 7876-7883. DOI: 10.1063/1.475100

[3] Shimamori, H.; Tatsumi, Y.; Ogawa, Y.; Sunagawa, T. Electron-energy dependence of electron attachment to c-C_7F_{14}, CH_3I and CH_2Br_2 studied by the pulse-radiolysis microwave-cavity technique combined with microwave heating. *Chem. Phys. Lett.* **1992**, *194*, 223-229. DOI: 10.1016/0009-2614(92)85539-M

[4] Parthasarathy, R.; Finch, C. D.; Wolfgang, J.; Nordlander, P.; Dunning, F. B. Low-energy dissociative electron attachment to CH_2Br_2, $CHClBr_2$, and CCl_3Br: Intermediate lifetimes and decay energetics. *J. Chem. Phys.* **1998**, *109*, 8829-8835. DOI: 10.1063/1.477553

[5] Nielsen, S. B.; Ayotte, P.; Kelley, J. A.; Weddle, G. H.; Johnson, M. A. Infrared spectra of hydrogen-bonded ion-radical complexes: $I^- \cdot HCH_2$ and $Br^- \cdot HCHBr$. *J. Chem. Phys.* **1999**, *111*, 10464-10468. DOI: 10.1063/1.480392

[6] Kim, J.; Kelley, J. A.; Ayotte, P.; Nielsen, S. B.; Weddle, G. H.; Johnson, M. A. Preparation and photoelectron spectrum of the CH_3I^- anion: Rare gas cluster mediated synthesis of an ion-radical complex. *J. Am. Soc. Mass Spectrom.* **1999**, *10*, 810-814. DOI: 10.1016/S1044-0305(99)00057-4

[7] Robertson, W. H.; Weddle, G. H.; Johnson, M. A. Strong similarities in the local hydration environments of the bromide ion and the $Cl^- \cdot CCl_3 \cdot$ ion-radical complex: Factors contributing to intramolecular distortions in the primary hydration shell. *J. Phys. Chem. A.* **2003**, *107*, 9312-9318. DOI: 10.1021/jp030641r

[8] Corkish, T. R.; Haakansson, C. T.; McKinley, A. J.; Wild, D. A. The structure of $CCl_5{}^-$ in the gas phase. *J. Phys. Chem. Lett.* **2019**, *10*, 5338-5342. DOI: 10.1021/acs.jpclett.9b02242

[9] Cavallo, G.; Metrangolo, P.; Milani, R.; Pilati, T.; Priimagi, A.; Resnati, G.; Terraneo, G. The halogen bond. *Chem. Rev.* **2016**, *116*, 2478-2601. DOI: 10.1021/acs.chemrev.5b00484

[10] Clark, T.; Heßelmann, A. The coulombic σ-hole model describes bonding in $CX_3I \cdots Y^-$ complexes completely. *Phys. Chem. Chem. Phys.* **2018**, *20*, 22849-22855. DOI: 10.1039/C8CP03079K

[11] Clark, T.; Murray, J. S.; Politzer, P. A perspective on quantum mechanics and chemical concepts in describing noncovalent interactions. *Phys. Chem. Chem. Phys* **2018**, *20*, 30076-30082. DOI: 10.1039/C8CP06786D

[12] Řezáč, J.; de la Lande, A. On the role of charge transfer in halogen bonding. *Phys. Chem. Chem. Phys.* **2017**, *19*, 791-803. DOI: 10.1039/C6CP07475H

[13] Thirman, J.; Engleage, E.; Huber, S. M.; Head-Gordon, M. Characterizing the interplay of Pauli repulsion, electrostatics, dispersion and charge transfer in halogen bonding with energy decomposition analysis. *Phys. Chem. Chem. Phys.* **2018**, *20*, 905-915. DOI: 10.1039/C7CP06959F

[14] Kunin, A.; McGraw, V. S.; Lunny, K. G.; Neumark, D. M. Time-resolved dynamics in iodide-uracil-water clusters upon excitation of the nucleobase. *J. Chem. Phys.* **2019**, *151*, 154304. DOI: 10.1063/1.5120706

[15] DeVine, J. A.; Babin, M. C.; Blackford, K.; Neumark, D. M. High-resolution photoelectron spectroscopy of the pyridinide isomers. *J. Chem. Phys.* **2019**, *151*, 064302. DOI: 10.1063/1.5115413

[16] Corkish, T. R.; 't Hart, D. B.; Watson, P. D.; McKinley, A. J.; Wild, D. A. Characterisation of gas phase halide-acetone complexes with photoelectron spectroscopy and *ab initio* calculations. *J. Mol. Spec.* **2019**, *364*, 111178. DOI: 10.1016/j.jms.2019.111178

[17] Corkish, T. R.; Haakansson, C. T.; McKinley, A. J.; Wild, D. A. Evidence for a water-stabilised ion radical complex: Photoelectron spectroscopy and *ab initio* calculations. *Aust. J. Chem.* **2020**, *73*, 693-698. DOI: 10.1071/CH19428

[18] Neumark, D. M. Slow electron velocity-map imaging of negative ions: Applications to spectroscopy and dynamics. *J. Phys. Chem. A.* **2008**, *112*, 13287-13301. DOI: 10.1021/jp807182q

[19] National Institute of Standards and Technology, *NIST Chemistry WebBook*, *NIST Standards Reference Database Number 69* **2018** (NIST: Gaithersburg, MD).

[20] Blondel, C.; Cacciani, P.; Delsart, C.; Trainham, R. High-resolution determination of the electron affinity of fluorine and bromine using crossed ion and laser beams. *Phys. Rev. A.* **1989**, *40*, 3698-3701. DOI: 10.1103/PhysRevA.40.3698

[21] Lapere, K. M. L.; Kettner, M.; Watson, P. D.; McKinley, A. J.; Wild, D. A. Halide-nitrogen gas-phase clusters: Anion photoelectron spectroscopy and high level ab initio calculations. *J. Phys. Chem. A.* **2015**, *119*, 9722-9728. DOI: 10.1021/acs.jpca.5b06348

[22] Markovich, G.; Giniger, M.; Levin, M.; Cheshnovsky, O. Photoelectron spectroscopy of negative ions solvated in clusters. *Z. Phys. D.* **1991**, *20*, 69-72. DOI: 10.1007/BF01543940

[23] Wiley, W. C.; McLaren, I. H. Time-of-flight mass spectrometer with improved resolution. *Rev. Sci. Instrum.* **1955**, *26*, 1150-1157. DOI: 10.1063/1.1715212

[24] Cheshnovsky, O.; Yang, S. H.; Pettiette, C. L.; Craycraft, M. J.; Smalley, R. E. Magnetic time-of-flight photoelectron spectrometer for mass-selected negative cluster ions. *Rev. Sci. Instrum.* **1987**, *58*, 2131-2137. DOI: 10.1063/1.1139475

[25] Lapere, K. M.; LaMacchia, R. J.; Quak, L. H.; McKinley, A. J.; Wild, D. A. Anion photoelectron spectroscopy and *ab initio* calculations of the gas phase chloride-carbon monoxide complex: $Cl^- \cdots CO$. *Chem. Phys. Lett.* **2011**, *504*, 13-19. DOI: 10.1016/j.cplett.2011.01.034

[26] Frisch, M. J.; Trucks, G. W.; Schlegel, H. B.; Scuseria, G. E.; Robb, M. A.; Cheeseman, J. R.; Scalmani, G.; Barone, V.; Mennucci, B.; Petersson, G. A.; Nakatsuji, H.; Caricato, M.; Li, X.; Hratchian, H. P.; Izmaylov, A. F.; Bloino, J.; Zheng, G.; Sonnenberg, J. L.; Hada, M.; Ehara, M.; Toyota, K.; Fukuda, R.; Hasegawa, J.; Ishida, M.; Nakajima, T.; Honda, Y.; Kitao, O.; Nakai, H.; Vreven, T.; Montgomery Jr., J. A.; Peralta, J. E.; Ogliaro, F.; Bearpark, M.; Heyd, J. J.; Brothers, E.; Kudin, K. N.; Staroverov, V. N.; Kobayashi, R.; Normand, J.; Raghavachari, K.; Rendell, A.; Burant, J. C.; Iyengar, S. S.; Tomasi, J.; Cossi, M.; Rega, N.; Millam, J. M.; Klene, M.; Knox, J. E.; Cross, J. B.; Bakken, V.; Adamo, C.; Jaramillo, J.; Gomperts, R.; Stratmann, R. E.; Yazyev, O.; Austin, A. J.; Cammi, R.; Pomelli, C.; Ochterski, J. W.; Martin, R. L.; Morokuma, K.; Zakrzewski, V. G.; Voth, G. A.; Salvador, P.; Dannenberg, J. J.; Dapprich, S.; Daniels, A. D.; Farkas, Ö.; Foresman, J. B.; Ortiz, J. V.; Cioslowski, J.; Fox, D. J. *Gaussian 09, Revision D.01,* Gaussian, Inc., Wallingford CT, 2013.

[27] Dunning, T. H. Gaussian basis sets for use in correlated molecular calculations. I. The atoms boron through neon and hydrogen. *J. Chem. Phys.* **1989**, *90*, 1007-1023. DOI: 10.1063/1.456153

[28] Kendall, R. A.; Dunning, T. H.; Harrison, R. J. Electron affinities of the first-row atoms revisited. Systematic basis sets and wave functions. *J. Chem. Phys.* **1992**, *96*, 6796-6806. DOI: 10.1063/1.462569

[29] Peterson, K. A.; Figgen, D.; Goll, E.; Stoll, H.; Dolg, M. Systematically convergent basis sets with relativistic psudopotentials. II. Small-core pseudopotentials and correlation consistent basis sets for the post-d group 16-18 elements. *J. Chem. Phys.* **2003**, *119*, 11113-11123. DOI: 10.1063/1.1622924

[30] Stanton, J. F.; Gauss, J.; Harding, M. E.; Szalay, P. G. CFOUR, Coupled-cluster techniques for computational chemistry.

[31] Karton, A.; Martin, J. M. L. Comment on: Estimating the hartree-fock limit from finite basis set calculations [Jensen F (2005) Theor Chem Acc 113:267]. *Theo. Chem. Acc.* **2006**, *115*, 330-333. DOI: 10.1007/s00214-005-0028-6

[32] Helgaker, T.; Klopper, W.; Kock, H.; Noga, J. Basis-set convergence of correlated calculations on water. *J. Chem. Phys.* **1997**, *106*, 9639-9646. DOI: 10.1063/1.473863

[33] Karton, A.; Rabinovich, E.; Martin, J. M. L.; Ruscic, B. W4 theory for computational thermochemistry:In pursuit of confident sub-$\mathrm{kJ/mol}$ predictions. *J. Chem. Phys.* **2006**, *125*, 144108. DOI: 10.1063/1.2348881

[34] Karton, A.; Martin, J. M. L. Explicitly correlated Wn theory: W1-F12 and W2-F12. *J. Chem. Phys.* **2012**, *136*, 124114. DOI: 10.1063/1.3697678

[35] Endo, Y.; Yamada, C.; Saito, S.; Hirota, E. The microwave spectrum of the fluoromethyl radical, CH_2F. *J. Chem. Phys.* **1983**, *79*, 1605-1611. DOI: 10.1063/1.446006

[36] Sears, T. J.; Temps, F.; Wagner, H. Gg.; Wolf, M. Far-infrared laser magnetic resonance spectroscopy of CH_2Cl ($\tilde{\chi}^2 B_1$). *J. Mol. Spec.* **1994**, *168*, 136-146. DOI: 10.1006/jmsp.1994.1266

[37] Bailleux, S.; Dréan, P.; Zelinger, Z.; Civiš, S.; Ozeki, H.; Saito, S. Millimeter wave spectrum of bromomethyl radical, CH_2Br. *J. Chem. Phys.* **2005**, *122*, 134302. DOI: 10.1063/1.1862619

[38] Ozeki, H.; Okabayashi, T.; Tanimoto, M.; Saito, S.; Bailleux, S. Hyperfine resolved spectrum of the bromomethyl radical, CH_2Br, by Fourier transform microwave spectroscopy. *J. Chem. Phys.* **2007**, *127*, 224301. DOI: 10.1063/1.2805187

[39] Bailleux, S.; Kania, P.; Skřínský, J.; Okabayashi, T.; Tanimoto, M.; Matsumoto, S.; Ozeki, H. Hyperfine resolved Fourier transform microwave and millimeter-wave spectroscopy of the iodomethyl radical, CH_2I ($\tilde{\chi}^2 B_1$). *J. Phys. Chem. A.* **2010**, *114*, 4776-4784. DOI: 10.1021/jp909323h

[40] Kortyna, A.; Lesko, D. M. B.; Nesbitt, D. J. High-resolution sub-Doppler infrared spectroscopy of atmopsherically relevant Ciregee precursor CH_2I radicals: CH_2 stretch vibrations and "charge sloshing" dynamics. *J. Chem. Phys.* **2018**, *148*, 174308. DOI: 10.1063/1.5028287

[41] Li, Z.; Francisco, J. S. High level *ab initio* molecular orbital study of the structures and vibrational spectra of CH_2Br and CH_2Br^+. *J. Chem. Phys.* **1999**, *110*, 817-822. DOI: 10.1063/1.478049

[42] Li, Q.; Zhao, J. Xie, Y.; Schaefer III, H. F. Electron affinities, molecular structures, and thermochemistry of the fluorine, chlorine and bromine substituted methyl radicals. *Mol. Phys.* **2002**, *100*, 3615-3648. DOI: 10.1080/00268970210000021804

[43] Marshall, P.; Srinivas, G. N.; Schwartz, M. A computational study of the thermochemistry of bromie- and iodine- containing methanes and methyl radicals. *J. Phys. Chem. A.* **2005**, *109*, 6371-6379. DOI: 10.1021/jp0518052

[44] Becke, A. D. Density-functional thermochemistry. III. The role of exact exchange. *J. Chem. Phys.* **1993**, *98*, 5648-5652. DOI: 10.1063/1.464913

[45] Goerigk, L.; Grimme, S. A thorough benchmark of density functional methods for general main group thermochemistry, kientics, and noncovalent interactions. *Phys. Chem. Chem. Phys.* **2011**, *13*, 6670-6688. DOI: 10.1039/C0CP02984J

[46] Arnold, D. W.; Bradforth, S. E.; Kim, E. H.; Neumark, D. M. Study of $I^-(CO_2)_n$, $Br^-(CO_2)_n$, and $I^-(N_2O)_n$ clusters by anion photoelectron spectroscopy. *J. Chem. Phys.* **1995**, *102*, 3510-3518. DOI: 10.1063/1.468576